
Since January 2020 Elsevier has created a COVID-19 resource centre with free information in English and Mandarin on the novel coronavirus COVID-19. The COVID-19 resource centre is hosted on Elsevier Connect, the company's public news and information website.

Radiation Physics and Chemistry 198 (2022) 110265

Contents lists available at ScienceDirect

Radiation Physics and Chemistry

journal homepage: www.elsevier.com/locate/radphyschem

# Inactivation of SARS-CoV-2 by charged particles for Future Vaccine Production Applications: A Monte Carlo study

Payman Rafiepour [a], Sedigheh Sina [a,b,*], Seyed Mohammad Javad Mortazavi [c,d]

[a] Department of Nuclear Engineering, School of Mechanical Engineering, Shiraz University, Shiraz, Iran
[b] Radiation Research Center, School of Mechanical Engineering, Shiraz University, Shiraz, Iran
[c] Department of Medical Physics and Engineering, School of Medicine, Shiraz University of Medical Sciences, Shiraz, Iran
[d] Ionizing and Non-ionizing Radiation Protection Research Center (INIRPRC), Shiraz University of Medical Sciences, Shiraz, Iran

ARTICLE INFO

*Keywords:*
Coronavirus
SARS-CoV-2
Vaccine
Monte Carlo
Geant4

ABSTRACT

The world is still suffering from the SARS-CoV-2 pandemic, and the number of infected people is still growing in many countries in 2022. Although great strides have been made to produce effective vaccines, efforts in this field should be accelerated, particularly due to the emergence of new variants. Using inactivated viruses is a conventional method of vaccine production. High levels of ionizing radiation can effectively inactivate viruses. Recently, studies on SARS-CoV-2 irradiation using low-LET radiations (e.g., gamma rays) have been performed. However, there are insufficient studies on the impact of charged particles on the inactivation of this virus. In this study, a realistic structure of SARS-CoV-2 is simulated by using Geant4 Monte Carlo toolkit, and the effect of electrons, protons, alphas, C-12, and Fe-56 ions on the inactivation of SARS-CoV-2 is investigated. The simulation results indicated that densely ionizing (high-LET) particles have the advantage of minimum number of damaged spike proteins per single RNA break. The RNA breaks induced by hydroxyl radicals produced in the surrounding water medium were significant only for electron beam radiation. Hence, indirect RNA breaks induced by densely ionizing particles is negligible. From a simulation standpoint, alpha particles (with energies up to 30 MeV) as well as C-12 ions (with energies up to 80 MeV/n), and Fe-56 ions (with any energy) can be introduced as particles of choice for effective SARS-CoV-2 inactivation.

## 1. Introduction

The severe acute respiratory syndrome coronavirus 2 (SARS-CoV-2) pandemic has been plaguing the world for more than two years, and its global incidence and mortality rates are increasing rapidly in many countries. According to the World Health Organization, as of September 1, 2021, the number of patients and deaths due to the new coronavirus was nearly 215 million and 4.5 million worldwide, respectively (World Health Emergency Dashboard, 2021). Due to the global outbreak of the virus and its high mortality rate, efforts to develop effective vaccines are still underway. On the other hand, the high rate of mutation and the alteration of SARS-CoV-2 protein structure adds to the concern of increasing their transmissibility and resistance to vaccines (Plante et al., 2021). Several studies have reviewed the rapid progress of vaccine development (Kaur and Gupta, 2020; Dong et al., 2020; Krammer, 2020). Using inactivated viruses is a conventional method of vaccine production, and the use of ionizing radiation such as gamma-rays has been reported as a convenient way to inactivate viruses (Sabbaghi et al., 2019; David et al., 2017; Elliott et al., 1982; Alsharifi and Müllbacher, 2010; Seo, 2015). To assist the studies related to the process of vaccine production, it is essential to study the effect of different ionizing radiations on the structure of SARS-CoV-2 with the aim of inactivation. Leung et al. experimentally determined the radiation dose required to inactivate SARS-CoV-2, using a Co-60 source (Leung et al., 2020). Although good results have been reported for the inactivation of viruses using X- or gamma ray irradiation, it should be further investigated in the case of SARS-CoV-2, due to possible mutations imposed by selective pressure (Mehdizadeh et al., 2020). Since laboratory facilities are not always available, Monte Carlo simulation is one of the best options for simulating statistical phenomena such as particle transport in matter.

*Abbreviations:* SARS-CoV-2, Severe acute respiratory syndrome coronavirus 2; RNA, Ribonucleic acid; DNA, Deoxyribonucleic acid; bp, base pair; LET, Linear-energy-transfer; PDB, Protein data bank; MeV/n, Mega electron-volt per nucleon.

* Corresponding author. Department of Nuclear Engineering, School of Mechanical Engineering, Shiraz University, Shiraz, Iran.
*E-mail address:* samirasina@shirazu.ac.ir (S. Sina).

https://doi.org/10.1016/j.radphyschem.2022.110265
Received 13 October 2021; Received in revised form 25 January 2022; Accepted 24 May 2022
Available online 28 May 2022

Using Monte Carlo methods, Zhang et al. carried out calculations of energy deposition and ionization on SARS-CoV-2 by electron beams of different energies (Zhang et al., 2020). Feng et al. extended similar calculations on SARS-CoV-2 including its surrounding environment (Feng et al., 2020). Both studies demonstrated the advantage of 1.5–2 keV electron beam irradiation to inactivate SARS-CoV-2. However, they acknowledged that the practical implementation would be difficult due to the very short range of electrons with such energies. Villagomez-Bernabe et al. simulated the SARS-CoV-2 structure with TOPAS Monte Carlo code, and investigated the effect of the 3D arrangement of the Ribonucleic acid (RNA) on survival curves (Villagomez-Bernabe et al., 2020). In a comprehensive study, Francis et al. simulated the SARS-CoV-2 inactivation caused by photons, electrons, and heavy ions using Geant4-DNA Monte Carlo code (Francis et al., 2021). They concluded that by considering the same damage to the RNA, densely ionizing or high-linear-energy-transfer (LET) radiation would be more advantageous in vaccine development due to their less damage to the spike proteins than that of sparsely ionizing (low-LET) radiation. However, more studies are needed on the impact of charged particles on SARS-CoV-2 inactivation. Since the samples of respiratory viruses are contained in viral aerosols, up to a few micrometers thick (Verreault et al., 2008), the effect of the medium should be considered. In this study, a more realistic structure of SARS-CoV-2 was simulated using a protein data bank (PDB) imported in Geant4-DNA. This structure which is placed inside a surrounding water medium, as the aerosol wall, was exposed to a beam of electrons, protons, alphas, and heavy ions such as C-12 and Fe-56. Several energies were examined for each radiation beam including 3 MeV, 10 MeV, 30 MeV, and 80 MeV for proton and alpha particles, and 25 MeV per nucleon (MeV/n), 80 MeV/n, 150 MeV/n, and 300 MeV/n for C-12 and Fe-56 ions. The frequency of damages in spike and RNA proteins induced by direct effects of such radiations as well as the relative survival curves were obtained, and being compared with each other. Furthermore, a simple modeling was performed to estimate the indirect damage to the RNA, induced by free radicals created in the virus, and the surrounding water medium.

## 2. Material and method

### 2.1. Geant4-DNA physical processes

Geant4 (version 10.7) Monte Carlo toolkit (Agostinelli et al., 2003) with the extension of Geant4-DNA (Incerti et al., 2010) was used to simulate the irradiation of SARS-CoV-2 structure with electrons, protons, alphas, and C-12 and Fe-56 ions. The default DNA physics-list class, "G4EmDNAPhysics_option2″, recommended for cellular and subcellular scale simulations (Bernal et al., 2015; Incerti et al., 2018), was implemented in this study. It includes several physics models that cover the physical interactions needed for particle transport in water. For electrons, the implemented physics models are G4DNABornExcitationModel, G4DNAChampionElasticModel, G4DNABornIonisationModel, G4DNAMeltonAttachmentModel, and G4DNASancheExcitation Model for electronic excitation, elastic scattering, ionization, molecular attachment, and vibrational excitation, respectively. The default energy cut for electrons is 7.4 eV, below which the transport of electrons would stop, and their remaining energy would be deposited locally. For protons, the implemented physics models are G4DNAIonElasticModel, G4DNAMillerGreenExcitationModel/G4DNABornExcitationModel, G4DNARuddIonisationModel/G4DNABornIonisationModel, and G4DNADingfelderChargeDecreaseModel for nuclear scattering, electronic excitation, ionization, and electron capture, respectively. For alphas, the implemented physics models are G4DNAIonElasticModel, G4DNAMillerGreenExcitationModel, G4DNARuddIonisationModel, and G4DNADingfelderChargeDecreaseModel for nuclear scattering, electronic excitation, ionization, and electron capture, respectively. For C-12 and Fe-56 ions, the implemented physics model is G4DNARuddIonisationExtendedModel for ionization. See (Bernal et al., 2015; Incerti et al., 2018) for the covering energy ranges as well as other available physics models. All these interactions take place in the physical stage, the first stage of the Geant4-DNA simulation process. Geant4-DNA has the capability of simulating chemical interactions through the physico-chemical and chemical stages (Karamitros et al., 2011). See (Karamitros et al., 2011, 2014) for the available chemical interactions, and the reaction rates of chemical species production which are implemented in Geant4-DNA. To simulate the chemical stage, the frequency of the chemical species ($OH^{\bullet}$, $H^{\bullet}$, $OH^{-}$, $H_2O^{+}$, $e^{-}_{aq}$, $H_3O^{+}$, $H_2O_2$) produced in the spherical water medium was obtained up to 1 ns after the beginning of the physical stage. Among the above-mentioned radicals, the frequency of hydroxyl radicals ($OH^{\bullet}$) is highly important due to the high risk of interactions with DNA molecules (Milligan et al., 1996).

### 2.2. SARS-CoV-2, source, and medium simulation

SARS-CoV-2, a member of Coronaviridae's family, is an enveloped virus that contains a single-stranded RNA packed inside the capsid. The capsid, surrounded by a membrane called the envelope, consists of nucleocapsid proteins. The membrane proteins, the envelope proteins, and the spike glycoproteins, are distributed on the envelope layer. Although viral genome replication is carried out by the RNA, the invasion of a human host cell, i.e., the onset of the SARS-CoV-2 infection, is carried out by the spike glycoproteins (Mariano et al., 2020). Therefore, destroying RNA sequence while keeping spikes less damaged is a key in the process of inactivation (Seo, 2015). The SARS-CoV-2 geometry simulated in Geant4 is shown in Fig. 1. The inner radius of the capsid and the envelope was set to 60 nm and 70 nm, respectively. Thus, the thickness of the envelope membrane was set to 10 nm. This is a typical radius obtained from the literature (Shereen et al., 2020). It should be noted that the diameter of SARS-CoV-2 ranges between 50 and 200 nm (Halim et al., 2021). Two PDB files with correspondent IDs of 6VXX and 6VYO were employed to construct spike and RNA structures, respectively (Mariano et al., 2020). The spike containers were represented as simple cylinders with ~13.1 nm diameter and ~19.4 nm height. To avoid overlapping of the spikes, only 147 spike containers were uniformly distributed on the surface of the envelope. For the simulation of RNA, the nucleocapsid proteins (ID: 6VYO) were positioned inside spherical containers with a radius of ~5.9 nm. The 6VYO protein structure consists of 499 residues and the viral RNA sequence length has been reported to be 29,903 base pairs (bps) (Khailany et al., 2020). As several studies have emphasized that the RNA genome of SARS coronavirus is wrapped with the nucleocapsid proteins (Chen et al., 2007; Cao et al., 2021), we defined a circular RNA segment of 110 bps that wraps around each container of the nucleocapsid proteins. Therefore, 50 spherical containers along with a circular RNA segment were randomly distributed inside the capsid volume to fulfill the desired number of bps. Each RNA bp is represented as a simple cylinder with a radius of 0.5 nm and a length of 0.34 nm. For modeling each sugar part of the RNA, a quarter cylinder was simulated with an inner and outer radius of 0.5 nm and 1.185 nm, respectively. Each quarter cylinder was rotated by 36° on the next bp to represent the helical shape of a single RNA strand. A zoomed-in view of this structure is shown in Fig. 1-b. In this section, the bps and the sugar parts are shown in blue and red, respectively. Although the only validated material in Geant4-DNA is water, the density (or the cross-section) scaling is allowable in Geant4-DNA. Utilizing the density scaling approach is a good approximation since the mean free path of electrons depends on the material's density (Shingledecker et al., 2020; Emfietzoglou et al., 2007). Thus, different densities were set for the water medium in the regions with a higher density than that of pure water. These regions include the spikes, the envelope, and the capsid with a density of 1.40 g/cm$^3$, 1.38 g/cm$^3$ and, 1.46 g/cm$^3$, respectively (Shingledecker et al., 2020; Emfietzoglou et al., 2007). The virus model was centered inside a spherical water medium

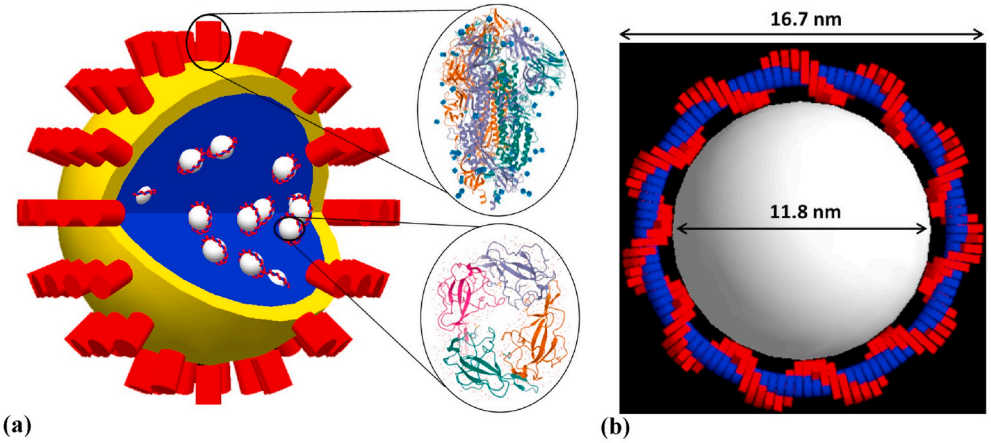


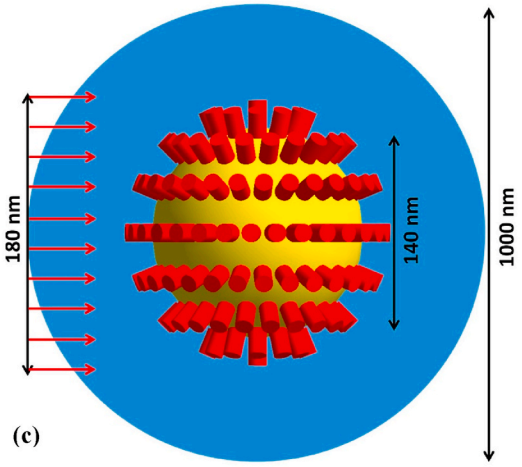


**Fig. 1.** a) The virus geometry including spike containers (red cylinders), and nucleocapsid protein containers (white spheres), each of which contains the corresponding PDB structures, i.e., 6VXX and 6VYO for spikes and RNA, respectively. The envelope and the capsid are shown in yellow and blue, respectively. See text for dimensions. **b)** A single nucleocapsid protein container with a wrapping RNA segment of 110 base pairs. **c)** The simulation of the source, and the surrounding medium of the virus. Dimensions are not on a correct scale.

with a radius of 500 nm. The primary particles were uniformly shot from the surface of a circular plane with a radius of 180 nm, 500 nm from the left-hand side of the virus geometry along the horizontal axis (see Fig. 1-c).

### 2.3. Damage calculations

The amount of energy depositions and their positions were recorded for each interaction of the primary and secondary particles with the spike proteins and RNA. Viruses cannot repair any damages in their RNA (or DNA) since they lack repair enzymes. Thus, a single RNA damage is sufficient to inactivate the virus. In this simulation, if the energy deposited in a single atom of the RNA (i.e., either in a residue of a nucleocapsid protein or in a bp of the wrapping RNA segments) was greater than 10.79 eV, the ionization energy threshold of water (Dingfelder et al., 1998), one damage is assumed to occur. This consideration helps us to estimate the virus survival curves. The target theory (Lea, 1947), the simplest model of cellular response to radiation, is best suited for describing the behavior of viruses under irradiation. The survival fraction is obtained by the following exponential equation (Wulf et al., 1985; Durante et al., 2020):

$$S = \exp(-\sigma F) \quad (1)$$

in which $\sigma$, the inactivation cross-section, is the probability multiplied by the cross-sectional surface of the RNA structure (i.e., the probability of a single RNA damage), and F is the fluence (particle/cm2) of incident particles, which is related to their deposited dose and LET (Wulf et al., 1985; Roots et al., 1990).

For estimating the indirect RNA breaks, we only consider $OH^{\bullet}$ as the most reactive radical. We assumed that each of the $OH^{\bullet}$ produced inside the bounding volume of the RNA (nucleocapsid containers plus the wrapping single strand RNA segments) would react with RNA proteins. Thus, the number and the locations of all $OH^{\bullet}$ produced in the RNA containers were recorded. Note that not all $OH^{\bullet}$ lead to the strand breaks. The probability of a single strand break due to the interaction of $OH^{\bullet}$ with the DNA has been shown to be 13%–22% (Scholes et al., 1969; Nikjoo et al., 1997). We assumed an average probability of 17.5% in our calculation.

The DNA damage yields are usually expressed per unit of dose, as well as the genome length (Neary et al., 1972; Charlton et al., 1989). Hence, the damage yield induced in the virus can be obtained by equation (2):

$$\text{Damage yield } \left(\text{Gy}^{-1}\text{kbp}^{-1}\right) = N_{break} / \left(D \times N_{bp}\right) \quad (2)$$

in which $N_{break}$ is the number of breaks, D is the total absorbed dose to the virus (Gy) and $N_{bp}$ (kbp) is the number of bps or the genome length in terms of kbps.

## 3. Results and discussion

The total energy deposited in all spike ($E_S$) and RNA ($E_R$) proteins in terms of eV/particle, as well as the relative frequency of ionizations and excitations that occurred in the spikes and RNA are tabulated in Tables 1 and 2. The frequency of ionizations and excitations is normalized to the number of primary particles. Increasing the incident energy results in lower energy depositions, since LET is inversely related to the kinetic energy of the primary particle. Total ionization included "e−_G4DNAIonisation", "proton_G4DNAIonisation", "alpha_G4DNA

**Table 1**
The frequency of ionization and excitation as well as the total energy deposited in the spikes ($E_S$) and RNA ($E_R$) per incident electrons, protons, and alphas.

| Incident particle | Energy (MeV) | Ionization in spikes | Excitation in spikes | Ionization in RNA | Excitation in RNA | $E_S$ (eV/particle) | $E_R$ (eV/particle) |
|---|---|---|---|---|---|---|---|
| Electron | 5e-3 | 0.064 | 0.353 | 0.009 | 0.050 | 1.25 | 0.179 |
| | 0.02 | 0.073 | 0.408 | 0.013 | 0.072 | 1.43 | 0.256 |
| | 0.2 | 0.022 | 0.123 | 0.003 | 0.018 | 0.434 | 0.066 |
| | 0.5 | 0.015 | 0.086 | 0.002 | 0.013 | 0.304 | 0.046 |
| Proton | 3 | 1.06 | 6.05 | 0.165 | 0.936 | 20.9 | 3.24 |
| | 10 | 0.374 | 2.11 | 0.054 | 0.312 | 7.40 | 1.07 |
| | 30 | 0.140 | 0.802 | 0.022 | 0.119 | 2.77 | 0.428 |
| | 80 | 0.062 | 0.336 | 0.010 | 0.051 | 1.21 | 0.192 |
| Alpha | 3 | 13.2 | 67.3 | 2.14 | 10.4 | 255 | 40.7 |
| | 10 | 4.86 | 23.7 | 0.713 | 3.52 | 94.5 | 13.9 |
| | 30 | 1.84 | 8.88 | 0.256 | 1.24 | 35.8 | 5.00 |
| | 80 | 0.832 | 3.94 | 0.112 | 0.523 | 14.7 | 2.16 |

**Table 2**
The frequency of ionization and excitation as well as the total energy deposited in the spikes ($E_S$) and RNA ($E_R$) per incident C-12 and Fe-56 ions.

| Incident particle | Energy (MeV/n) | Ionization in spikes | Excitation in spikes | Ionization in RNA | Excitation in RNA | $E_S$ (eV/particle) | $E_R$ (eV/particle) |
|---|---|---|---|---|---|---|---|
| C-12 | 25 | 5.81 | 26.6 | 0.857 | 4.23 | 110 | 16.6 |
| | 80 | 2.12 | 10.0 | 0.323 | 1.45 | 40.3 | 6.12 |
| | 150 | 1.31 | 6.31 | 0.204 | 0.99 | 25.1 | 3.88 |
| | 300 | 0.836 | 3.92 | 0.123 | 0.572 | 16.1 | 2.34 |
| Fe-56 | 25 | 108 | 545 | 14.1 | 74.0 | 2048 | 273 |
| | 80 | 41.5 | 198 | 5.16 | 23.2 | 796.3 | 98.7 |
| | 150 | 23.9 | 116 | 3.51 | 18.4 | 457.8 | 66.5 |
| | 300 | 15.9 | 74.9 | 2.13 | 10.7 | 301.9 | 40.5 |
| | 1000 | 8.91 | 43.0 | 1.28 | 6.10 | 170.9 | 24.6 |

Ionisation", "alpha+_G4DNAIonisation", and "GenericIon_G4DNAIonisation" processes, and total excitation included "e−_G4DNAExcitation", "proton_G4DNAExcitation", "alpha_G4DNAExcitation", "alpha+_G4DNAExcitation", and "e−_G4DNAVibExcitation" processes which are implemented in Geant4-DNA (Bernal et al., 2015; Incerti et al., 2018). Note that most of the excitation frequency was due to the process of vibrational excitation, i.e., "e−_G4DNAVibExcitation". However, this physical process may not significantly affect the total energy deposition in the virus (Brunger et al., 2016).

Fig. 2 plots the direct damage yield in all spike and RNA proteins obtained by equation (2), for five incident particles. Three initial energies were considered for electrons (5 keV, 20 keV, and 200 keV), protons (3 MeV, 10 MeV, and 30 MeV), alphas (3 MeV, 10 MeV, and 30 MeV), C-12 ions (25 MeV/n, 80 MeV/n, and 150 MeV/n), and Fe-56 ions (150 MeV/n, 300 MeV/n, and 1 GeV/n). A high damage yield in the RNA is favorable, provided that a minimal damage to the spikes occurs, simultaneously. Therefore, the number of damaged spikes normalized per single RNA damage is interesting. We are looking for a radiation field that causes the least number of damaged spikes per single RNA break as suggested by (Durante et al., 2020; Francis et al., 2021) for the first time. This ratio is represented in Fig. 3 for different incident particles. Fig. 4 shows possibly desirable radiations for SARS-CoV-2 inactivation, which cause less than 2 damaged spikes per single RNA break. The LET values of primary particles in water were obtained from Geant4 database.

As shown in Fig. 3, the number of damaged spikes per RNA break increases as the initial energy of incident particle increases. The lowest number of damaged spikes normalized to a single RNA break was 0.06 for Fe-56 ions of 25 MeV/n energy (LET = 1455 keV/μm), followed by 0.18, and 0.36 for Fe-56 ions of 80 MeV/n energy (LET = 585.4 keV/μm), and alpha particles of 3 MeV (LET = 125.6 keV/μm), respectively. Therefore, densely ionizing particles (high-LET) such as alphas, and C-12 and Fe-56 ions seem to be more advantageous for a 'clean' inactivation of SARS-CoV-2 than electrons and protons. This benefit is also shown in Fig. 4. Fig. 4 indicates a strong LET (i.e., track structure) dependence, which is similar to what observed for the inactivation of

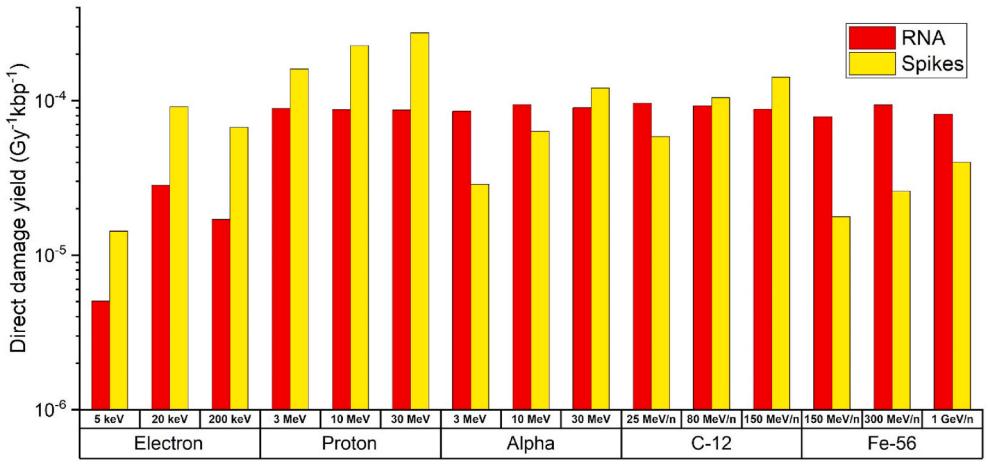


**Fig. 2.** The normalized direct damage induced in the spikes and the RNA, by five incident particles with different energies, obtained by equation (2).

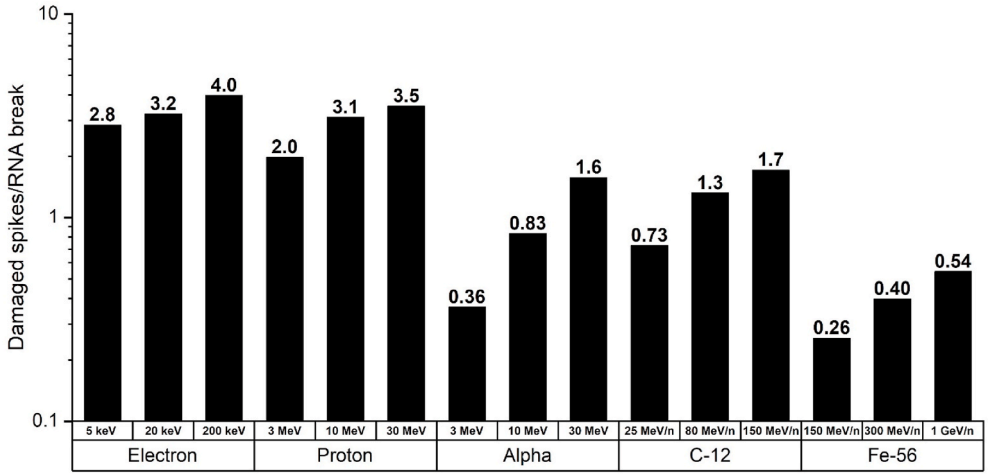


**Fig. 3.** The number of damaged spikes normalized to a single RNA break for different incident particles with different energies.

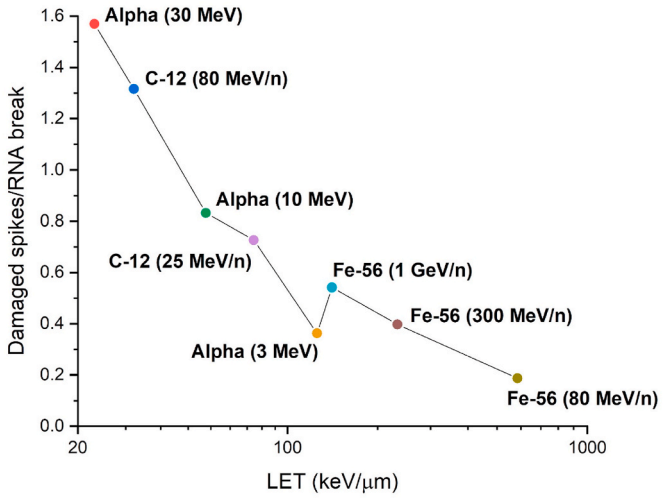


**Fig. 4.** The number of damaged spikes normalized to a single RNA break as a function of linear-energy-transfer (LET) for some favorable incident particles for SARS-CoV-2 inactivation.

mammalian cells (Wulf et al., 1985; Blakely, 1992; Suzuki et al., 1996). It has been shown that the inactivation cross-section increases non-linearly with increasing LET (Tsuruoka et al., 2005; Belloni et al., 2002; Wulf et al., 1985; Blakely, 1992). It is worth noting that for mammalian cells, the mechanisms of cell repair play an important role in shaping the cell survival curve, and leads to complicated radiobiological responses (Heilmann et al., 1993; Okayasu, 2012). Fig. 4 demonstrates that the maximum initial energy of alpha particles and C-12 ions should not exceed 30 MeV and 80 MeV/n, respectively. In contrast, there is no energy limit for Fe-56 ions, since a single Fe-56 ion may be sufficient for SARS-CoV-2 inactivation.

Fig. 5 shows the frequency of indirect RNA breaks due to the reaction of $OH^{\bullet}$ with RNA molecules, normalized to the genome length as well as the unit of dose delivered to the virus by the incident particle. Three initial energies were considered for each particle type. The relative ratio of direct and indirect RNA damages is shown in Fig. 6.

As shown in Figs. 5 and 6, the yield of indirect damages is significant for electrons (low-LET). The increase in indirect damages with decreasing LET is similar to the results reported for mammalian cells (Roots et al., 1985, 1990). By comparing Figs. 2 and 5, one can infer that most of RNA damages are induced by direct effects for high-LET particles and the opposite is true for low-LET particles, i.e. electrons. This is consistent with the results published in the literature (Hirayama et al., 2009; Yamashita et al., 2008; Ito et al., 2006). However, the relationship between the ratio of direct/indirect RNA damage and the LET of incident

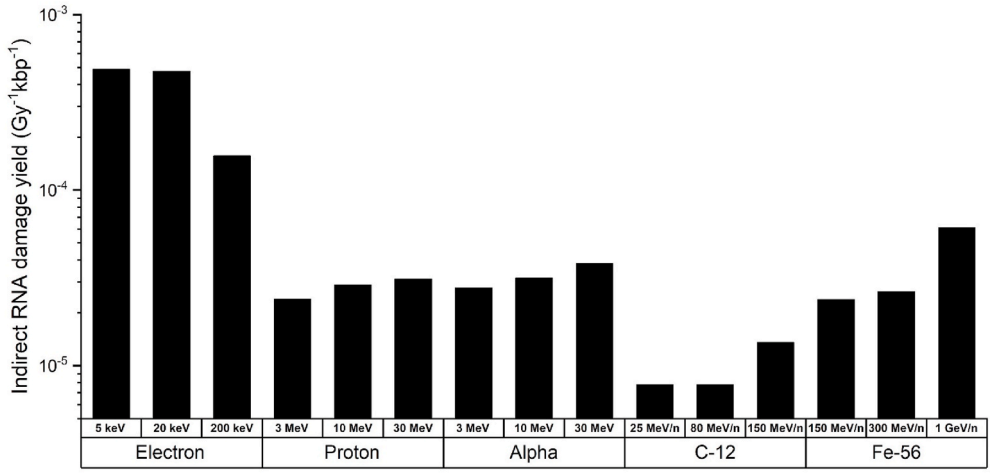


**Fig. 5.** The normalized indirect RNA breaks due to reaction of $OH^{\bullet}$ with RNA molecules, obtained by equation (2). Three initial energies were considered for each particle type.

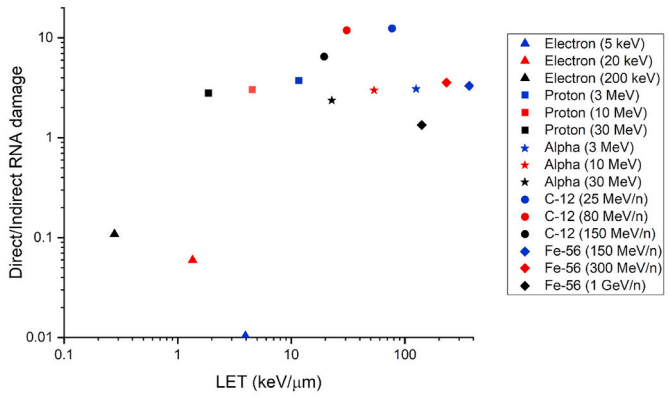


**Fig. 6.** The relative ratio of direct and indirect RNA breaks due to reaction of $OH^{\bullet}$ with RNA molecules versus the LET of incident particles.

particles does not follow a specific trend, which means that LET alone may not be a determining factor in choosing the best particle for SARS-CoV-2 inactivation. The highest value for the ratio of direct and indirect RNA damages was 12.3 for 25 MeV/n C-12 ions, while the lowest value was 0.01 for 5 keV electrons. Due to the advantage of densely ionizing particles (see Fig. 3), we ignored the indirect radiation effects. In addition, the virus inactivation is performed in the freezing condition that leads to a large reduction of indirect effects. However, a comparison of the frequency of $OH^{\bullet}$ within the volume of the RNA containers for different primary particles could be interesting.

The estimated survival curves of SARS-CoV-2 obtained by equation (1), for several incident particles are shown in Fig. 7. The type of particles was selected from Fig. 4.

The survival curves indicate that high-LET radiations require a larger dose to inactivate SARS-CoV-2. This is consistent with the results of the previous study by Francis et al. (2021), however, the data are not quantitatively the same. This may be due to differences in geometry of SARS-CoV-2. Note that only the probability of occurring at least one RNA break was considered in equation (1). In other words, the impact of selective pressure induced by radiation is not taking into account in survival curves of viruses. As mentioned before, the impact of indirect RNA breaks was not also considered in Fig. 7, due to the insignificance of indirect effects for high-LET radiations.

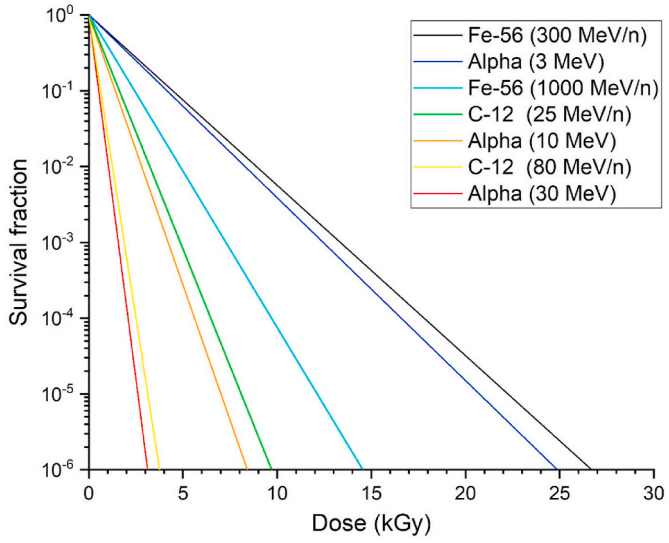


**Fig. 7.** The survival curves of SARS-CoV-2 obtained by equation (1), for different primary particles.

## 4. Conclusion

In this study, a comparison of five primary charged particles (electron, proton, alpha, and C-12 and Fe-56 ions) with different energies was performed for the inactivation of SARS-CoV-2 using Geant4 Monte Carlo toolkit. From a simulation standpoint, the optimal energy of incident particles for the aim of SARS-CoV-2 inactivation, should be the energy for which the number of damaged spike proteins normalized to a single RNA break is minimum. This is achieved for densely ionizing (high-LET) radiations. The results indicated that alpha particles with a maximum energy of 30 MeV, C-12 ions with a maximum energy of 80 MeV/n, and Fe-56 ions with any typical energy are more interesting for the inactivation of SARS-CoV-2 than electrons and protons. Nevertheless, the availability and the practical issues with accelerating heavy charged particles should be taken into account, which needs further studies.

## Ethics approval and consent to participate

Not applicable.

## Consent for publication

Not applicable.

## Availability of data and materials

All data produced from this study will be available from the corresponding author on reasonable request.

## Funding

None.

## Authors' contributions

Payman Rafiepour: Methodology, Software, Validation, Formal analysis, Investigation, Writing - Original Draft. Sedigheh Sina: Methodology, Investigation, Resources, Writing - Review & Editing, Supervision, Project administration. Seyed Mohammad Javad Mortazavi: Conceptualization, Methodology, Investigation, Writing - Review & Editing, Supervision.

## Author statement

We declare that the manuscript titled as "*Inactivation of SARS-CoV-2 by charged particles for Future Vaccine Production Applications: A Monte Carlo study*" is original, has not been published before and is not currently being considered for publication elsewhere.

We confirm that the manuscript has been read and approved by all named authors and that there are no other persons who satisfied the criteria for authorship but are not listed.

We further confirm that the order of authors listed in the manuscript has been approved by all of us. We understand that the Corresponding Author is the sole contact for the Editorial process, and is responsible for communicating with the other authors about progress, submissions of revisions and final approval of proofs.

## Declaration of competing interest

The authors declare that they have no known competing financial interests or personal relationships that could have appeared to influence the work reported in this paper.

## Acknowledgment

None.

## References


Agostinelli, S., Allison, J., Amako, K., Apostolakis, J., Araujo, H., Arce, P., et al., 2003. Geant4—a simulation toolkit. Nucl. Instruments Methods Phys. Res. Sect. A Accel. Spectrometers, Detect. Assoc. Equip. 506, 250–303. https://doi.org/10.1016/S0168-9002(03)01368-8.

Alsharifi, M., Müllbacher, A., 2010. The gamma-irradiated influenza vaccine and the prospect of producing safe vaccines in general. Immunol. Cell Biol. 88 (2), 103–104. https://doi.org/10.1038/icb.2009.81.

Belloni, F., Bettega, D., Calzolari, P., Cherubini, R., Massariello, P., Tallone, L., 2002. Inactivation cross sections for mammalian cells exposed to charged particles: a phenomenological approach. Radiat. Protect. Dosim. 99 (1–4), 199–202. https://doi.org/10.1093/oxfordjournals.rpd.a006761.

Bernal, M.A., Bordage, M.C., Brown, J., Davídková, M., Delage, E., El Bitar, Z., et al., 2015. Track structure modeling in liquid water: a review of the Geant4-DNA very low energy extension of the Geant4 Monte Carlo simulation toolkit. Phys. Med. 31 (8), 861–874. https://doi.org/10.1016/j.ejmp.2015.10.087.

Blakely, E.A., 1992. Cell inactivation by heavy charged particles. Radiat. Environ. Biophys. 31 (3), 181–196. https://doi.org/10.1007/BF01214826.

Brunger, M., Ratnavelu, K., Buckman, S., et al., 2016. Investigating the role of vibrational excitation in simulating charged-particle tracks in liquid pyrimidine. Eur. Phys. J. D 70, 46. https://doi.org/10.1140/epjd/e2016-60641-8.

Cao, C., Cai, Z., Xiao, X., et al., 2021. The architecture of the SARS-CoV-2 RNA genome inside virion. Nat. Commun. 12, 3917. https://doi.org/10.1038/s41467-021-22785-x.

Charlton, D.E., Nikjoo, H., Humm, J.L., 1989. Calculation of initial yields of single- and double-strand breaks in cell nuclei from electrons, protons and alpha particles. Int. J. Radiat. Biol. 56 (1), 1–19. https://doi.org/10.1080/09553008914551141.

Chen, C.Y., Chang, C.K., Chang, Y.W., Sue, S.C., Bai, H.I., Riang, L., Hsiao, C.D., Huang, T.H., 2007. Structure of the SARS coronavirus nucleocapsid protein RNA-binding dimerization domain suggests a mechanism for helical packaging of viral RNA. J. Mol. Biol. 368 (4), 1075–1086. https://doi.org/10.1016/j.jmb.2007.02.069.

David, S.C., Lau, J., Singleton, E.V., Babb, R., Davies, J., Hirst, T.R., et al., 2017. The effect of gamma-irradiation conditions on the immunogenicity of whole-inactivated Influenza A virus vaccine. Vaccine 35 (7), 1071–1079. https://doi.org/10.1016/j.vaccine.2016.12.044.

Dingfelder, M., Hantke, D., Inokuti, M., Paretzke, H.G., 1998. Electron inelastic-scattering cross-sections in liquid water. Radiat. Phys. Chem. 53, 1–18. https://doi.org/10.1016/S0969-806X(97)00317-4.

Dong, Y., Dai, T., Wei, Y., et al., 2020. A systematic review of SARS-CoV-2 vaccine candidates. Signal Transduct. Targeted Ther. 5, 237. https://doi.org/10.1038/s41392-020-00352-y.

Durante, M., Schulze, K., Incerti, S., Francis, Z., Zein, S., Gzman, C.A., 2020. Virus irradiation and COVID-19 disease. Front. Physiol. 8 (565861), 1–8.

Elliott, L.H., McCormick, J.B., Johnson, K.M., 1982. Inactivation of lassa, marburg, and Ebola viruses by gamma irradiation. J. Clin. Microbiol. 16 (4), 704–708. https://doi.org/10.1128/JCM.16.4.704-708.1982.

Emfietzoglou, D., Nikjoo, H., Pathak, A., Sathish, N., 2007. A comparison of secondary electron spectra from proton-impact ionization on water in the liquid and solid phases. Nucl. Instrum. Methods Phys. Res., Sect. B 257, 609–613. https://doi.org/10.1016/j.nimb.2007.01.049.

Feng, G., Liu, L., Cui, W., et al., 2020. Electron beam irradiation on novel coronavirus (COVID-19): a Monte–Carlo simulation. Chin. Phys. B 29 (4), 048703. https://doi.org/10.1088/1674-1056/ab7dac.

Francis, Z., Incerti, S., Zein, S.A., et al., 2021. Monte Carlo simulation of SARS-CoV-2 radiation-induced inactivation for vaccine development. Radiat. Res. 195 (3), 221–229. https://doi.org/10.1667/rade-20-00241.1.

Halim, F.S., Parmin, N.A., Hashim, U., Gopinath, S.C.B., Dahalan, F.A., Zakaria, I.I., et al., 2021. MicroRNA of N-region from SARS-CoV-2: potential sensing components for biosensor development. Biotechnol. Appl. Biochem. 1 https://doi.org/10.1002/bab.2239. –16.

Heilmann, J., Rink, H., Taucher-Scholz, G., Kraft, G., 1993. DNA strand break induction and rejoining and cellular recovery in mammalian cells after heavy-ion irradiation. Radiat. Res. 135 (1), 46–55.

Hirayama, R., Ito, A., Tomita, M., Tsukada, T., Yatagai, F., Noguchi, M., Matsumoto, Y., Kase, Y., Ando, K., Okayasu, R., Furusawa, Y., 2009. Contributions of direct and indirect actions in cell killing by high-LET radiations. Radiat. Res. 171 (2), 212–218. https://doi.org/10.1667/RR1490.1.

Incerti, S., Baldacchino, G., Bernal, M.A., Capra, R., Champion, C., Francis, Z., et al., 2010. The GEANT4-DNA project. Int. J. Model. Simulation, Sci. Comput. 1, 157–178.

Incerti, S., Kyriakou, I., Bernal, M.A., Bordage, M.C., Francis, Z., Guatelli, S., et al., 2018. Geant4-DNA example applications for track structure simulations in liquid water: a report from the Geant4-DNA Project. Med phys. https://doi.org/10.1002/mp.13048, 10.1002/mp.13048. Advance online publication.

Ito, A., Nakano, H., Kusano, Y., Hirayama, R., Furusawa, Y., Murayama, C., Mori, T., Katsumura, Y., Shinohara, K., 2006. Contribution of indirect action to radiation-induced mammalian cell inactivation: dependence on photon energy and heavy-ion LET. Radiat. Res. 165 (6), 703–712. https://doi.org/10.1667/RR3557.1.

Karamitros, M., Luan, S., Bernal, M.A., Allison, J., et al., 2014. Diffusion-controlled reactions modeling in Geant4-DNA. Comput. Phys. 274, 841–882. https://doi.org/10.1016/j.jcp.2014.06.011.

Karamitros, M., Mantero, A., Incerti, S., Friedland, W., et al., 2011. Modeling radiation chemistry in the Geant4 toolkit. Progr. Nucl. Sci. Technol. 2, 503–508. https://doi.org/10.15669/pnst.2.503.

Kaur, S.P., Gupta, V., 2020. COVID-19 Vaccine: a comprehensive status report. Virus Res. 288, 198114. https://doi.org/10.1016/j.virusres.2020.198114.

Khailany, R.A., Safdar, M., Ozaslan, M., 2020. Genomic characterization of a novel SARS-CoV-2. Gene reports 19, 100682. https://doi.org/10.1016/j.genrep.2020.100682.

Krammer, F., 2020. SARS-CoV-2 vaccines in development. Nature 586 (7830), 516–527. https://doi.org/10.1038/s41586-020-2798-3.

Lea, D.E., 1947. Action of Radiations on Living Cells. Cambridge University Press, New York, NY.

Leung, A., Tran, K., Audet, J., et al., 2020. In vitro inactivation of SARS-CoV-2 using gamma radiation. Appl Biosaf 25 (3), 157–160. https://doi.org/10.1177/1535676020934242.

Mariano, G., Farthing, R.J., Lale-Farjat, S., Bergeron, J., 2020. Structural characterization of SARS-CoV-2: where we are, and where we need to Be. Front. Mol. Biosci. 7, 605236. https://doi.org/10.3389/fmolb.2020.605236.

Mehdizadeh, A.R., Bevelacqua, J.J., Mortazavi, S.A.R., Mortazavi, S.M.J., 2020. COVID-19: introducing low dose radiation as an effective treatment for pneumonia that shouldn't induce selective pressure and new mutations. J Biomed Phys Eng 10 (3), 247–250. https://doi.org/10.31661/jbpe.v0i0.2005-1114.

Milligan, J.R., Wu, C.C., Ng, J.Y., Aguilera, J.A., Ward, J.F., 1996. Characterization of the reaction rate coefficient of DNA with the hydroxyl radical. Radiat. Res. 146 (5), 510–513.

Neary, G.J., Horgan, V.J., Bance, D.A., Stretch, A., 1972. Further data on DNA strand breakage by various radiation qualities. Int. J. Radiat. Biol. Relat. Stud. Phys. Chem. Med. 22 (6), 525–537. https://doi.org/10.1080/09553007214551431.

Nikjoo, H., O'Neill, P., Goodhead, D.T., Terrissol, M., 1997. Computational modelling of low-energy electron-induced DNA damage by early physical and chemical events. Int. J. Radiat. Biol. 71 (5), 467–483. https://doi.org/10.1080/095530097143798.

Okayasu, R., 2012. Repair of DNA damage induced by accelerated heavy ions–a mini review. Int. J. Cancer 130 (5), 991–1000. https://doi.org/10.1002/ijc.26445.

Plante, J.A., Liu, Y., Liu, J., Xia, H., Johnson, B.A., Lokugamage, K.G., et al., 2021. Spike mutation D614G alters SARS-CoV-2 fitness. Nature 592 (7852), 116–121. https://doi.org/10.1038/s41586-020-2895-3.

Roots, R., Chatterjee, A., Chang, P., Lommel, L., Blakely, E.A., 1985. Characterization of hydroxyl radical-induced damage after sparsely and densely ionizing irradiation. Int. J. Radiat. Biol. Relat. Stud. Phys. Chem. Med. 47 (2), 157–166. https://doi.org/10.1080/09553008514550231.

Roots, R., Holley, W., Chatterjee, A., Irizarry, M., Kraft, G., 1990. The formation of strand breaks in DNA after high-LET irradiation: a comparison of data from in vitro and cellular systems. Int. J. Radiat. Biol. 58 (1), 55–69. https://doi.org/10.1080/09553009014551431.

Sabbaghi, A., Miri, S.M., Keshavarz, M., Zargar, M., Ghaemi, A., 2019. Inactivation methods for whole infuenza vaccine production. Rev. Med. Virol. 29 (6), e2074 https://doi.org/10.1002/rmv.2074.

Scholes, G., Willson, R.L., Ebert, M., 1969. Pulse radiolysis of aqueous solutions of Deoxyribonucleotides and of DNA: reaction with hydroxy-radicals. Chem.Commun. 17–18. https://doi.org/10.1039/C29690000017.

Seo, H.S., 2015. Application of radiation technology in vaccines development. Clin Exp Vaccine Res 4 (2), 145–158. https://doi.org/10.7774/cevr.2015.4.2.145.

Shereen, M.A., Khan, S., Kazmi, A., Bashir, N., Siddique, R., 2020. COVID-19 infection: origin, transmission, and characteristics of human coronaviruses. J. Adv. Res. 24, 91–98. https://doi.org/10.1016/j.jare.2020.03.005.

Shingledecker, C.N., Incerti, S., Ivlev, A., Emfietzoglou, D., et al., 2020. Cosmic-ray tracks in astrophysical ices: modeling with the Geant4-DNA Monte Carlo toolkit. Astrophys. J. 904, 189. https://doi.org/10.3847/1538-4357/abbb30.

Suzuki, M., Watanabe, M., Kanai, T., Kase, Y., Yatagai, F., Kato, T., Matsubara, S., 1996. LET dependence of cell death, mutation induction and chromatin damage in human cells irradiated with accelerated carbon ions. Adv. Space Res. 18 (1–2), 127–136. https://doi.org/10.1016/0273-1177(95)00799-k.

Tsuruoka, C., Suzuki, M., Kanai, T., Fujitaka, K., 2005. LET and ion species dependence for cell killing in normal human skin fibroblasts. Radiat. Res. 163 (5), 494–500. https://doi.org/10.1667/rr3360.

Verreault, D., Moineau, S., Duchaine, C., 2008. Methods for sampling of airborne viruses. Microbiol. Mol. Biol. Rev.: MMBR (Microbiol. Mol. Biol. Rev.) 72 (3), 413–444. https://doi.org/10.1128/MMBR.00002-08.

Villagomez-Bernabe, B., Chan, S.W., Coulter, J.A., Roseman, A., Currell, F., 2020. Fast ion beam inactivation of viruses, where radiation track structure meets RNA structural biology. bioRxiv 8 (24), 265553. https://doi.org/10.1101/2020.08.24.265553, 2020.

WHO World Health Emergency Dashboard. (COVID-19) Homepage. https://covid19.who.int. (Accessed 1 September 2021).

Wulf, H., Kraft-Weyrather, W., Miltenburger, H.G., Blakely, E.A., Tobias, C.A., Kraft, G., 1985. Heavy-ion effects on mammalian cells: inactivation measurements with different cell lines. Radiat. Res. Suppl. 8, S122–S134. https://doi.org/10.2307/3576639.

Yamashita, S., Katsumura, Y., Lin, M., Muroya, Y., Maeyama, T., Murakami, T., 2008. Water radiolysis with heavy ions of energies up to 28GeV—2: extension of primary yield measurements to very high LET values. Radiat. Phys. Chem. 77 (10), 1124–1229. https://doi.org/10.1016/j.radphyschem.2008.05.037.

Zhang, X., Wang, F., Weng, M., Cao, M., 2020. Calculations of energy deposition and ionization in the 2019 novel coronavirus by electron beam irradiation. Radiat Phys Chem Oxf Engl 1993 177, 109169. https://doi.org/10.1016/j.radphyschem.2020.109169.